Bulletin of the Seismological Society of America, Vol. 92, No. 5, pp. 1721–1736, June 2002

A Comparative Study of the Sumatran Subduction-Zone Earthquakes of 1935 and 1984

by Luis Rivera, Kerry Sieh, Don Helmberger, and Danny Natawidjaja

Abstract A M_s 7.7 earthquake struck the western, equatorial coast of Sumatra in December 1935. It was the largest event in the region since the two devastating giant earthquakes of 1833 and 1861. Historical seismograms of this event from several observatories around the world provide precious information that constrains the source parameters of the earthquake. To more precisely quantify the location, geometry, and mechanism of the 1935 event and to estimate the coseismic deformation, we analyze the best of the available teleseismic historical seismograms by comparing systematically the records of the 1935 earthquake with those of a smaller event that occurred in the same region in 1984. First we constrain the source parameters of the 1984 event using teleseismic records. Then, we compare the records of the 1935 event with those of 1984 from the same sites and instruments. To do this, we choose several time windows in the corresponding seismograms that contain clearly identifiable phases and deconvolve the modern event from the older one. The deconvolutions result in very narrow pulses with similar sizes, thus confirming similar locations and mechanisms for the events. The initiation of the 1984 event was on the subduction interface at a depth of 27 $\pm$ 2 km; its M_0 is 6.5 $\times$ 10^{19} N m (M_w is 7.2). The sense of slip was nearly pure thrust, on a plane dipping 12°. The 1935 event also involved rupture of the shallow subduction interface, but was about five times larger (M_0 3.3 $\times$ 10;^{20} N m, M_w 7.7) and initiated a few kilometers to the southeast, along strike. The 1935 rupture propagated unilaterally toward the southeast. The along-strike rupture length was about 65 km. From these source parameters, we calculate the surface deformations, assuming an elastic multilayered medium. These deformations compare favorably with those actually recovered from paleoseismic data in the form of coral microatolls.

Introduction

Significance

Oblique subduction beneath Sumatran plate boundary has resulted in large earthquakes in 1935 and 1984. These major earthquakes are particularly interesting because they occurred at or near the juncture of two long sections of the Sumatran subduction zone that produced even larger earthquakes in the nineteenth century (Fig. 1). Historical accounts of shaking and tsunamis constrain the sources of the giant earthquakes of 1833 and 1861 to sections, several hundred kilometers in length, of the subduction interface southeast and northwest of the Equator (Newcomb and McCann, 1987). The sources of the 1935 and 1984 earthquakes are near the Equator, in the vicinity of the subducting Investigator Fracture Zone (Gutenberg and Richter, 1954; Engdahl *et al.*, 1998).

Coral microatoll stratigraphy and geomorphology constrain the source of the 1833 earthquake further. Models of coral uplift and tilt a few hundred kilometers south of the Equator yield more than 10 m of dip slip on the shallow-dipping subduction interface and suggest that the magnitude of the earthquake was between M_w 8.8 and 9.2 (Zachariasen *et al.*, 1999). We are still in the process of constraining the displacements and geographic extents of the 1833 event and its predecessors with paleoseismic data, in an attempt to understand the repetition of very large earthquakes. We are also using paleoseismic records to understand the behavior of the subduction zone in the region where the giant 1833 and 1861 ruptures appear to have abutted.

Is there a persistent segment boundary for giant earthquakes in this region of the smaller 1935 and 1984 events? How do the sources of smaller earthquakes, like the 1935 and 1984 events, relate to those of the larger events? Are the 1935 and 1984 earthquakes on the subduction interface, or do they represent failure of the overriding plate or fragmentation of the downgoing slab, like the recent (4 June 2000)

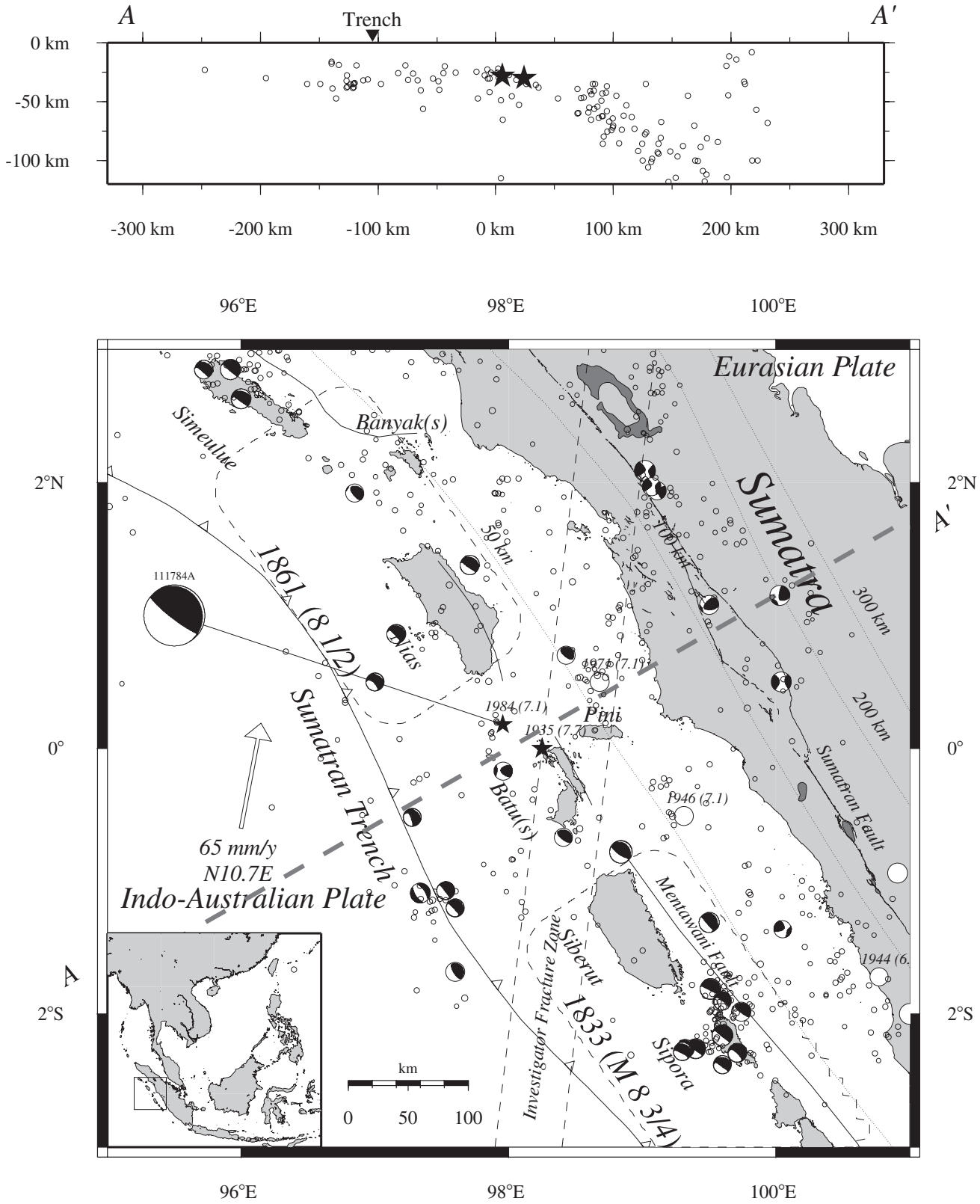
A
Trench
A′
0 km
-50 km
-100 km
-300 km
-200 km
-100 km
0 km
100 km
200 km
300 km
96°E
98°E
100°E
2°N
0°
2°S
Eurasian Plate
Simeulue
Banyak(s)
Nias
Pini
Batu(s)
Siberut
Sipora
Mentawai Fault
Sumatra
Sumatran Fault
Sumatran Trench
Investigator Fracture Zone
Indo-Australian Plate
65 mm/y
N10.7E
1861 (8 1/2)
1833 (M 8 3/4)
1984 (7.1)
1935 (7.7)
1946 (7.1)
1944 (6.
111784A
50 km
100 km
200 km
300 km
km
0
50
100

Figure 1. Source of the 1935 *M* 7.7 earthquake, situated between the much larger source regions of the giant *M* 8¾ and 8½ earthquakes of 1833 and 1861. The Investigator Fracture Zone (IFZ) is subducting beneath Sumatra at about this location. Source region of the earlier subduction events is modified from Zachariasen *et al.* (1999) and Newcomb and McCann (1987). Epicenter of the 1935 earthquake is from Gutenberg and Richter (1954). Epicenter of the 1984 earthquake is from Engdahl *et al.* (1998). ISC-relocated earthquakes from 1964–1998, Harvard centroid moment tensor $M_w \geq 5.5$, The triangles indicate the position of the trench. The contours of the Benioff zone are indicated with dotted lines. The epicenters of 1935 and 1984 are shown as stars. Large white circles represent the large and great shallow events from 1903 to 1985 (Newcomb and McCann, 1987). The arrow on the left bottom part of the figure indicate the relative motion at latitude 0° of the Indo-Australian plate with respect to the Eurasian plate. The prolongation of the IFZ within the subduction is indicated with dotted lines. Cross section centered at (0N, 98E), 200 km width, showing the ISC-relocated seismicity, the position of the trench, and the location of the 1984 and 1935 events.

event several hundred kilometers further southeast (Abercrombie *et al.*, 2000). If they were produced by slip on the subduction interface, are they pure dip-slip, do they recur, and does enough slip occur to account for all of the 40 to 50 mm/yr of dip slip across the subduction interface (Sieh *et al.*, 1999)? How do the source parameters of these earthquakes relate to strain accumulation measured in the decades before and after the events? These are questions that can be addressed with paleoseismic records, if we can first characterize seismologically the 1935 and 1984 events.

In the region of the 1935 and 1984 earthquakes, we have also recovered paleogeodetic records of uplift and submergence from the stratigraphic record of living coral microatolls. These data suggest that, for at least the past 30 years, the subduction interface has been primarily locked above depths of about 35 km (Sieh *et al.*, 1999). Geodetic Global Positioning System (GPS) measurements in the early 1990s, however, suggest that this section of the subduction interface is slipping wholly or in large part aseismically (Prawirodirdjo *et al.*, 1997). This is the geological setting, then, for this seismological study of two of the largest instrumentally recorded events in the region.

In this work, we analyze several teleseismic seismograms of the 1935 Sumatran earthquake in order to quantify the location, geometry, and mechanism of the event. Historical seismograms preserved in several observatories around the world are precious pieces of information that can help to span the gap between the modern and preinstrumental period. Previous studies have demonstrated the importance and the usefulness of historical seismograms (e.g., Bolt, 1968; Okal, 1977; Hartzell and Helmberger, 1982; Kanamori, 1988; Helmberger *et al.*, 1992; Wald *et al.*, 1993; Estabrook *et al.*, 1994; Cummins *et al.*, 2001; Doser and Brown, 2001). This is especially true when other independent informations (for example, historic, paleoseismic, or paleogeodetic) are available to help constrain source parameters. These, in combination with space geodetic data (GPS; very long baseline interferometry, VLBI; and interferometric synthetic aperture radar, InSAR), which permit the estimation of short-term strain rates, should lead to a multidisciplinary approach to the problem of seismic hazard assessment.

After an analysis of the seismograms, we calculate vertical displacements from elastic dislocation modeling, to enable a comparison of our seismological results with paleoseismic observations that we plan to present in a future paper.

Neotectonic Setting

The Sumatran plate boundary trends northwest; however, the vector of relative plate motion (65 mm/yr) between the Indo-Australian plate and the South-East Asian plate is oriented about N10E (Prawirodirdjo *et al.*, 1997; Sieh *et al.*, 1999). Thus, relative motion between the plates is highly oblique, with both a convergent and a right-lateral component (Fig. 1). To a large degree, the right-lateral and convergent components are partitioned into two separate fault systems (Fitch, 1972). Convergence occurs predominantly across the subduction zone (McCaffrey, 1992). Seismicity and focal mechanisms show that the subduction interface is very shallow and dips gradually down-dip from near-horizontal at the trench to about 15°, 200 km landward. The convergent component on the interface is 40 to 45 mm/yr (Sieh *et al.*, 1999).

The right-lateral component of slip occurs predominantly on two faults in the over-riding plate (Fig. 1) (Sieh and Natawidjaja, 2000). The most prominent of these faults is the 2000-km-long Sumatran fault, which runs along the mountainous western backbone of the island. Dextral slip rates on this fault are 10 to 30 mm/yr (Sieh *et al.*, 1994). Another long fault, between the trench and the Sumatran fault, is the Mentawai Fault. Diament *et al.* (1992) interpret seismic reflection profiles across this submarine structure to indicate that it is predominately strike-slip, although its position along the eastern flank of the outer-arc ridge indicates that it or related structures must have had a significant component of dip slip in the Pliocene (Sieh and Natawidjaja, 2000). Minor disarticulation of the downgoing oceanic slab is also occurring along north-striking strike-slip faults (Deplus *et al.*, 1998), like the one that produced at least part of the M_w 7.8 earthquake of June 2000 beneath the subduction interface (Abercrombie *et al.*, 2000). These faults parallel the topographic grain of the subducting seafloor. One of the largest of these north-trending features on the seafloor, the Investigator Fracture Zone (IFZ), intersects the trench at the Equator and is subducting beneath the region of the 1935 and 1984 earthquakes. Beneath the subduction interface, the northward projection of the IFZ is illuminated by a level of

seismicity far higher than in the surrounding regions (Fauzi *et al.*, 1996).

Seismicity of the Sumatran Arc

An important study of the seismic history of the Sumatran subduction zone was made by Newcomb and McCann (1987). They found that the seismic activity of Sumatra was largely underestimated, due to the lack of big earthquakes during the instrumental period. They documented two giant earthquakes during the last century: one M_w 8¾ in 1833 and one M_w 8½ in 1861). They estimated these to have rupture lengths of 550 and 300 km, respectively. They also constructed, from historical archives, maps of the source zones for 26 historical earthquakes associated with subduction between 1681 and 1921.

Until the event in June 2000, the largest earthquake near the Sumatran subduction zone since 1861 was the 1935 event that we study herein. Gutenberg and Richter (1954) give a magnitude of M_s 7.9 for this event. Geller and Kanamori (1977) revised the magnitude downward to M_s 7.7, based on their inspection of Gutenberg's original notes. Another important but slightly smaller event occurred farther north in 1907. Its magnitude was M_s 7.6, and it produced a tsunami that devastated the island of Simeulue (Newcomb and McCann, 1987) (Fig. 1).

The top of Figure 1 shows a vertical cross section of the seismicity in a 200-km-wide band orthogonal to the trench. The coordinates are from the ISC-relocated catalog (Engdahl *et al.*, 1998), which contains events from 1964 to 1998. The pattern very clearly defines the geometry of the subduction zone. This information was used by Gundmundsson and Sambridge (1998) to construct a 3D model of the Benioff zone, whose contours are shown as dotted lines in the lower part of the figure. The Benioff zone dips gently ($\delta \sim 10°$) near the trench and under the outer-arc and steepens to the northeast.

The Harvard centroid moment tensor (CMT) focal mechanism solutions from 1976 to the present for events with $M_w \geq 5.5$ are also shown. The thrust events are mainly located offshore of Sumatra, with very shallowly east-dipping fault planes. Some dextral strike-slip events on a plane striking ~160°N occur along the trace of the Sumatran fault.

The M_w 7.1 event of November 1984 occurred close to the location of the 1935 earthquake. Both epicenters (Gutenberg and Richter, 1954; Engdahl *et al.*, 1998) appear as stars in Figure 1, along with the CMT solution for the modern shock. Below, we use the 1984 event as an empirical Green's function to analyze the seismograms of the 1935 event. For this reason, we start with a detailed review of the data from the modern event.

Modeling the Body Waves of the 1984 Event

Data and Method

The data used in this section for the 1984 Sumatra event are the teleseismic waveforms archived at IRIS DMC between 30° and 100° of the epicenter. The instrument responses appear in Figure 2; they are fairly homogeneous and correspond to the SRO, ASRO, or DWWSSN instruments, with a maximum sensitivity around 20 sec and for most of them (SRO) a sharp notch filter at 5 sec. The sampling frequency is 1 sample per second (sps).

The instrumental response is first deconvolved from each trace to obtain the ground displacement, using a tapering in frequency between 100 sec and 8 sec. A window of 80 sec around the *P* arrival is used from each vertical component and a window of the same duration is selected, after rotation, from the transverse component containing the *S* arrival. Those waveforms are used as data for the inversion procedure.

We use the algorithm developed by Kikuchi and Kanamori (1982, 1986, 1991), in which the source is discretized both in space and time and the moment mechanism of each elementary source is determined iteratively by fitting the residual seismograms.

First, all the necessary Green's functions (GFs) for the whole set of source–station combinations are calculated and stored. In this particular case, the GFs combine the propagator matrix technique (Haskell, 1964) for near-surface propagation (both near the source and near the station) and the ray theory approximation for the deep segment of propagation.

Once the GFs are available, two complementary approaches are used in the actual inversion. In the first approach, designed to study the focal mechanism and the directivity of the source, the azimuth of a horizontal line of sources is fixed and an inversion is made to obtain the history of the rupture and the mechanism associated with each elementary source. In the second approach, aimed at recovering the spatial distribution of the rupture, a plane of sources with

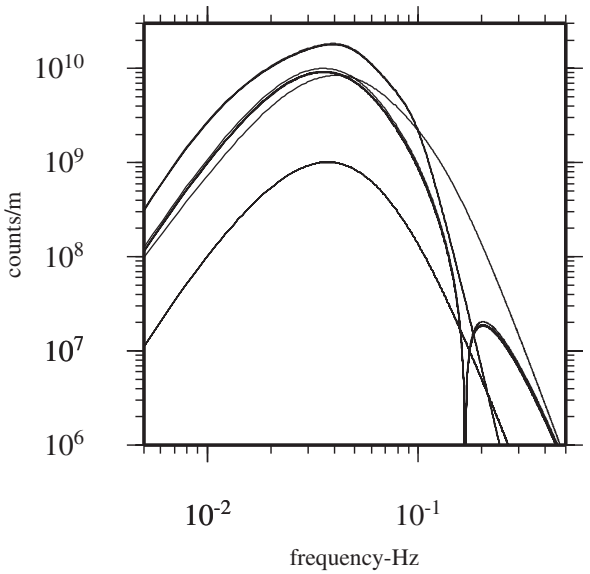

Figure 2. Instrumental responses for the instruments used in the source inversion for the 1984 event (DWWSSN, SRO, and ASRO networks).

a given focal mechanism is fixed and an inversion is performed to obtain the spatiotemporal distribution of the elementary sources within the given plane. The history of the source is modeled as the superposition of triangular functions with coefficients to be determined by the inversion.

In the case of a shallow-dipping fault plane like the Sumatran subduction zone, this last method is not very efficient in sampling different depths; hence, it was necessary to perform a set of inversions with different focal depths.

Velocity Model

For the near-source region we use the velocity model of Kieckhefer (1980), obtained from refraction data of the INDOPAC experiment in 1977. Specifically, we use his profile INDP: 1304-1305, shot between the Batu Islands and Nias. The model contains four layers, which are 1, 2, 17, and 20 km thick and which have P velocities of 2.5, 3.6, 4.9, and 7.5 km/sec, respectively. The P velocity in the half-space is $V_p = 8.1$ km/sec. The V_p/V_s ratio in all the layers is 1.73.

Results

To take into account the uncertainties in the velocity model near the source, we perform several inversions, with variations about the Kieckhefer model and with different reference depths. In all the cases more than about 80% of the seismic moment release was confined to a region smaller than or equal to 15 km, appearing essentially as a point source, given the spatial resolution that we can achieve with the periods used here. A similar argument about the spatial resolution could be applied to the depth, which fluctuated between 20 and 30 km, depending on the model; however, an independent and much more robust estimation of the depth can be obtained from the pP–P delays as measured in short-period teleseismic records (ATU, 8.0 sec; STU, 9.7 sec; KEV, 8.5 sec), which implies a hypocenter depth of 27 ± 2 km.

The triangles used to model the source–time function are 4 sec wide, in accordance with the highest-frequency content of the data. The total time span of the rupture history is about 16 sec; a simple triangle-shaped source–time function (Fig. 3) explains the waveforms fairly well. The duration is nearly invariant in the different inversions, even when a maximal source duration of 80 sec was allowed. The seismic moment is 6.5×10^{19} N m (M_w 7.2), about 10% higher than the Harvard CMT value (Dziewonski *et al.*, 1985). The main component of the focal mechanism represents a nearly pure thrust with a very shallow plane dipping to the northeast ($\phi = 332°$, $\delta = 12°$, $\lambda = 108°$). This orientation is very similar to the Harvard CMT solution ($\phi = 334°$, $\delta = 10°$, $\lambda = 116°$).

Several of the stations used in the inversion are nodal either in P (TOL, BCAO, TAXU) or in SH (COL, MAJO), (Fig. 3). These data provide particularly stringent constraints on the focal mechanism. The P-nodal stations constrain the dip of the fault plane. The slip direction is constrained by the S waveforms, since any rotation of the mechanism about a vertical axis will strongly affect the S amplitudes, as can be seen in the lower part of Figure 3.

The very low dip (δ) angle in this particular geometry introduces a strong trade-off between the strike (ϕ) and the rake (λ). In fact, in the extreme case of a horizontal plane, the variable $\phi + \lambda$ is completely unresolved (and meaningless); whereas the variable $\phi - \lambda$ bears the key information about the slip direction and completely determines the mechanism. Nevertheless, it seems that even the small value for the dip (10°–12°) is enough to allow resolution of the strike; in fact, those values of strike represent the local trend of the trench (330°) fairly well. The azimuth of the slip direction is 44°N in our solution and 38°N in the CMT solution. This convergence direction is halfway between the plate convergence and the normal to the trench. This event thus contributes mainly to the down-dip convergence, but also to the right-lateral displacement. This observation of imperfect partitioning was already made by Beck (1991) and McCaffrey (1992). Those authors elaborate on mechanical models to explain why both faults should participate in accommodating the lateral displacement, in the case of oblique convergence with two parallel faults (a vertical and a dipping one) delimiting a sliver plate.

In the Harvard solution, the duration of the source is fixed at an empirical value based on M_0; 27 sec in this case, almost double the duration that we propose. Certainly the real duration of the source of this event is far smaller than the resolution corresponding to the long periods used in calculating the CMT solutions (Dziewonski and Woodhouse, 1983). Even though the seismic moment differs only by 10%, the *potency* (Surface*Displacement $= M_0/\mu$; Ben Menahem and Singh, 1981) obtained here is significantly larger than in the CMT solution, 1.15 versus 0.86 km^3, as a result of the difference between the rigidity models used in each case. This difference is important because it is in fact this number and not the moment that will control the amplitude of the displacement field (Heaton and Heaton, 1989).

The amplitude of the signals (Fig. 3) correlates very well with the radiation patterns, and there is no evidence for directivity. The simplicity of the 1984 event in time and space and the absence of directivity justify the use of this event as a Green's function for the study of the 1935 earthquake.

The 1935 Earthquake

A large number of seismological stations were operating by 1935. The International Seismological Summary bulletin (ISS, 1946) lists about 200 stations reporting P or S arrival times for this event. The azimuthal coverage is rather poor, however, with a strongly bimodal distribution defined by the European stations around 320°N and East Asian and North American stations around 40°N. The arrival times are given in the summary for 1935 (ISS, 1946) as integer seconds, presumably corresponding to the optimal precision in time

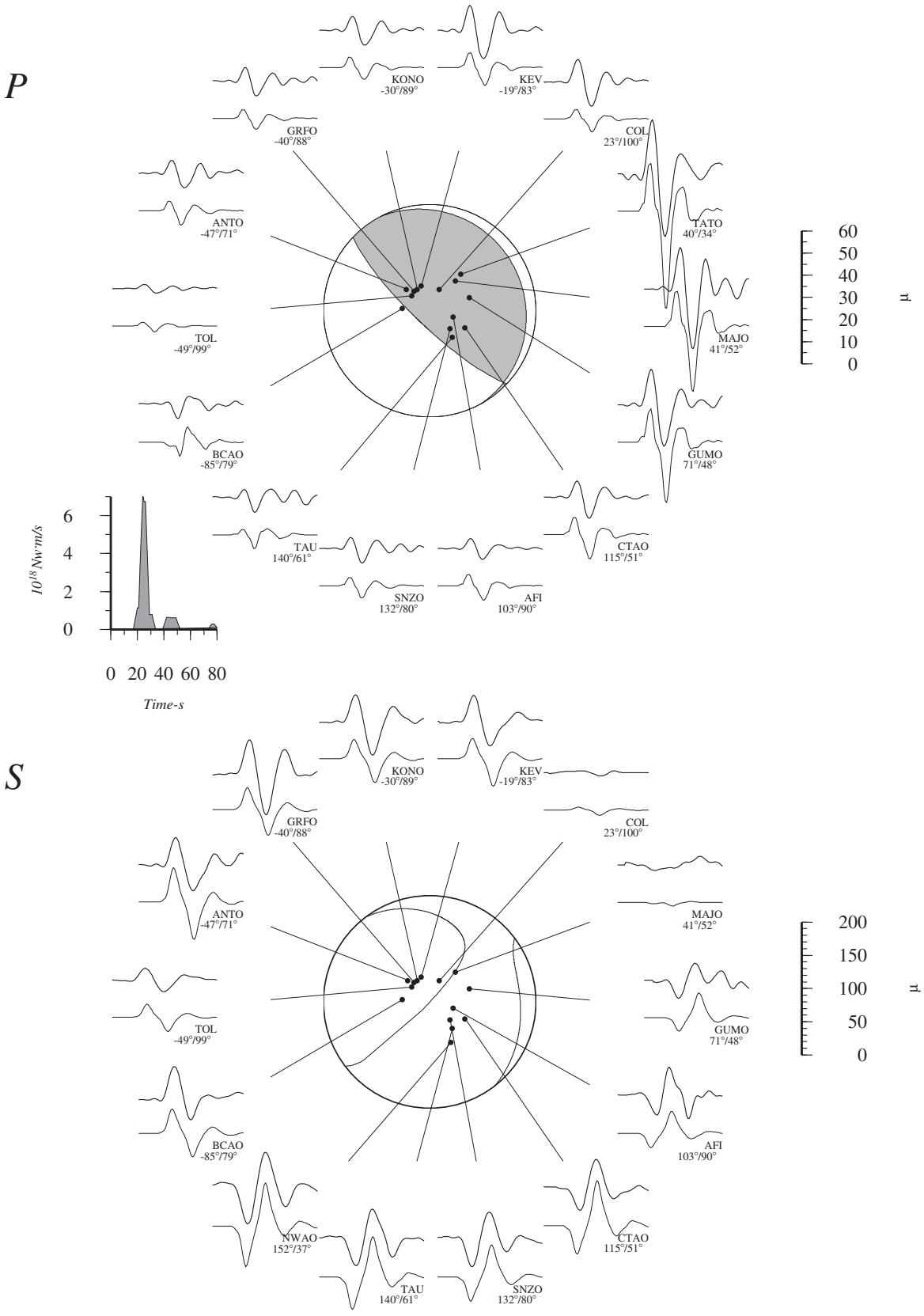

Figure 3. Result of the source inversion for the 1984 event. *P* and *SH* radiation patterns corresponding to $M_0 = 6.5 \times 10^{19}$ N m, $\phi = 332°$, $\delta = 12°$, and $\lambda = 108°$. The seismograms represent the ground displacement; the data are represented with the heavier line. The time scale in the seismograms is the same as that shown in the source time history, the amplitude axis is graduated in micrometers.

for a standard observatory around 1935. The residuals of the *P*-arrival times of this event in the ISS can be characterized by a root mean square (rms) value of 3 sec (discarding obviously wrong or contaminated residuals higher than 6 sec, the *pP–P* delay being ~7–8 sec). All those considerations, along with a mean horizontal *P* slowness of 7–8 sec/° for distances in the range 0°–100°, allow us to set a spatial resolution for the ISS location of this event of about 1/2°.

The epicenter reported by the ISS is 0.3°S and 97.9°E. Gutenberg and Richter (1954) relocated this event 30 km to the northeast (0°S and 98 1/4°E). They estimated their precision to be 1/4° both in latitude and longitude (about 30 km). The 1984 event was originally located by the ISC at 0.20°N and 98.03°E. Engdahl *et al.* (1998) relocated it at 0.18°N and 97.955°E. This relocation puts the epicenter of the 1984 event inside the confidence region of the Gutenberg–Richter location. Furthermore, the distance between both relocated epicenters is 35–40 km, comparable to the estimated dimension of the 1984 event and probably much smaller than the 1935 rupture. The two ruptures thus seem to be very close to each other.

Data: Historical Seismograms and Instruments

In spite of the large number of arrival times listed in the ISS catalog, we found very few independent seismograms to study this earthquake. In this study, we use records from four seismological stations: De Bilt, Netherlands (DBN); Wellington, New Zealand (WEL); Honolulu, Hawaii (HON); and College, Alaska (COL). Those stations also recorded the 1984 event, either at the same place and instrument (DBN) or within a few kilometers (10 km for HON; 3 km for WEL, at SNZO; 6 km for COL). The location of those four stations and the epicenter of the 1935 event are shown in Figure 4. For stations DBN and WEL we had access to 1:1 paper copies of the original records; for HON and COL, the records were available as microfilm.

Table 1 summarizes the characteristics of the four historical instruments used in this study and Figure 5 shows both the time-domain response of the instruments (the trace due to a delta-function force pulse) and the amplitude of their displacement response spectrum. The stations COL, HON, and WEL have very similar behavior; their displacement response is flat at high frequency and decays as f^2 at low frequency, and their periods are the same (12 sec). The instrument of DBN differs in that its amplitude response decays as f^{-1} at high frequency and as f^2 for low frequency, and it has a longer period and a higher damping.

Method: 1984 as a Green's Function for 1935

We digitize all the records at 2–4 samples/mm, equivalent roughly to 1–2 sec/sample. The minute marks of each record are also digitized, and a linear stretching is applied within each minute to the time axis to take into account the variable speed of the recording drum. The time series so obtained are then interpolated to 10 samples/sec and band-pass-filtered between 0.01 and 0.25 Hz. The length of the digitized traces ranges from 10 to 25 min, depending on the length of the available record, on the signal-to-noise ratio, and on our ability to clearly separate superposed traces. This digitization procedure is applied to the following set of records: 1935-DBN-EW/NS, 1935-COL-EW/NS, 1935-HON-EW/NS, 1935-WEL-EW/NS and 1984-DBN-EW/NS, which is completed with the digital records 1984-COL-EW/NS, 1984-HON-EW/NS and 1984-WEL-EW/NS from IRIS DMC. Hence, the complete set contains the two horizontal components for both events recorded at each of the four stations. These 16 time series comprise the data set used for the comparative study of the 1935 and 1984 events. The original traces are nearly naturally rotated, since the back azimuths are as follows: COL. N292°; DBN. N87°; HON. N275°; WEL. N279°. The E–W components are quasilongitudinal and the N–S are quasitransverse for all stations. A rotation of the historical digitized records to pure radial and transverse components did not improve the signal-to-noise ratio, so we decided to compare directly the original records: North-1935 with North-1984 and East-1935 with East-1984.

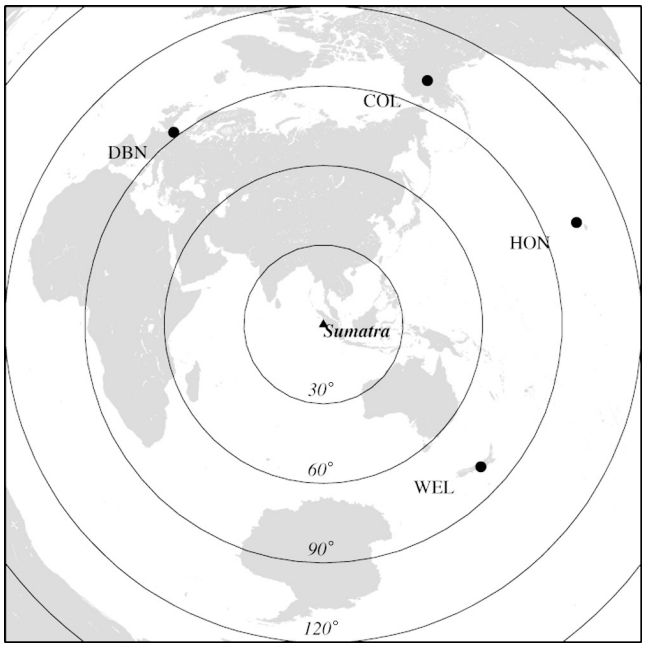

Figure 4. Distribution of the four stations used in the analysis of the 1935 event with respect to the epicenter: Honolulu, De Bilt, College, and Wellington.

Before doing the actual comparison of the records, the instrumental response has to be taken into account. Instead of deconvolving each record with its own response, we use a method based on the intercorrelation technique developed and applied by Lay *et al.* (1984) to yield estimation. The difference here is that we apply the procedure to the instrumental responses instead of the estimated source–time function. For each component at each station, we convolve the record of the 1935 event with the instrumental response of the corresponding record for 1984 and vice versa. The convolution being a commutative operation, the resulting traces contain the same equivalent instrument and can be directly compared.

Table 1
Characteristics of Four Historical Instruments

Station Name	De Bilt	Wellington	College	Honolulu
Code	DBN	WEL	COL	HON
Latitude/ Longitude	52.10°/5.18°	−41.31°/174.70°	64.90°/−147.79°	21.32°/−158.00°
Azim./Back Az./Dist.	322°/87°/92°	132°/279°/80°	23°/292°/100°	68°/275°/103°
Instrument type	Galitzine	Milne–Shaw	McComb–Romberg	Milne–Shaw
Paper speed (mm/min)	30	8	15	15
Magnification	319	250	140	150
Period (sec)	$T_g = T_s = 25$	12	12	12
Damping	$\xi_g = \xi_s = 1$	6:1	10:1	20:1
Bibliography	Savarensky and Kirnos, 1955; Macelwane and Sohon, 1932	Charlier and Van Gils, 1953	McComb, 1931; Romberg, 1919	Charlier and Van Gils, 1953; Peters, 1939

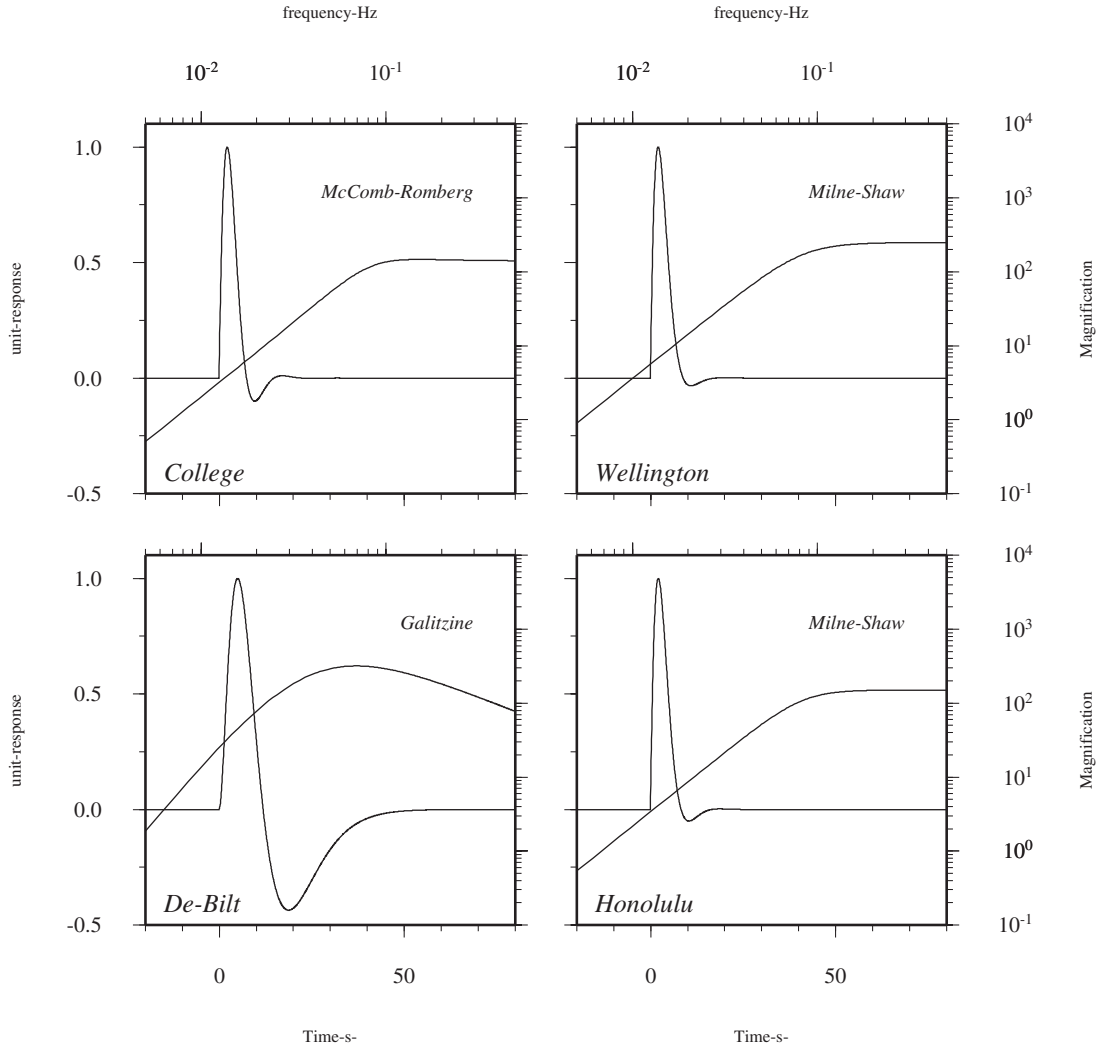

Figure 5. Response of the historical instruments used in this work. For each station, two independent plots are superposed: the time response to a dirac in force (simulating the calibration pulse) and the amplitude of the displacement response.

The next step is to measure the extent to which the 1935 records can be explained by a convolution of the corresponding 1984 trace (Green's function) and a source–time function. With this aim, we first choose the phases that appear clearly on both traces and, for each one of them, we deconvolve the 1984 phase from the corresponding one in 1935. The propagation and instrumental effects being the same in both traces, the result of the deconvolution has to be interpreted in terms of the source–time function of the 1935 event with respect with the 1984 one.

Results

Figure 6 shows the traces after instrument reconvolution. The traces corresponding to the 1984 event are plotted with a scale four times bigger than the traces of 1935, to illustrate better their similarity. Also, each trace is accompanied by an inset showing its first segment amplified eight times. The theoretical arrival times for phases clearly appearing in both traces have been identified; when several phases arrive grouped in time, the most energetic one is used to name the packet. A duration of 100 to 150 sec was used in the deconvolution, depending on the width of the phase.

A clear pulse appears in the deconvolution for most of the phases in at least one of the two components. The deconvolutions fall into four groups. Three of them (A, B, and C) correspond to different qualities of the deconvolution (dark circles, dark triangles, and light circles in Fig. 8). The fourth group (D) contains the cases corresponding to diffracted phases (shown with crosses in Fig. 8). The best deconvolutions for each station are shown in Figure 7. The

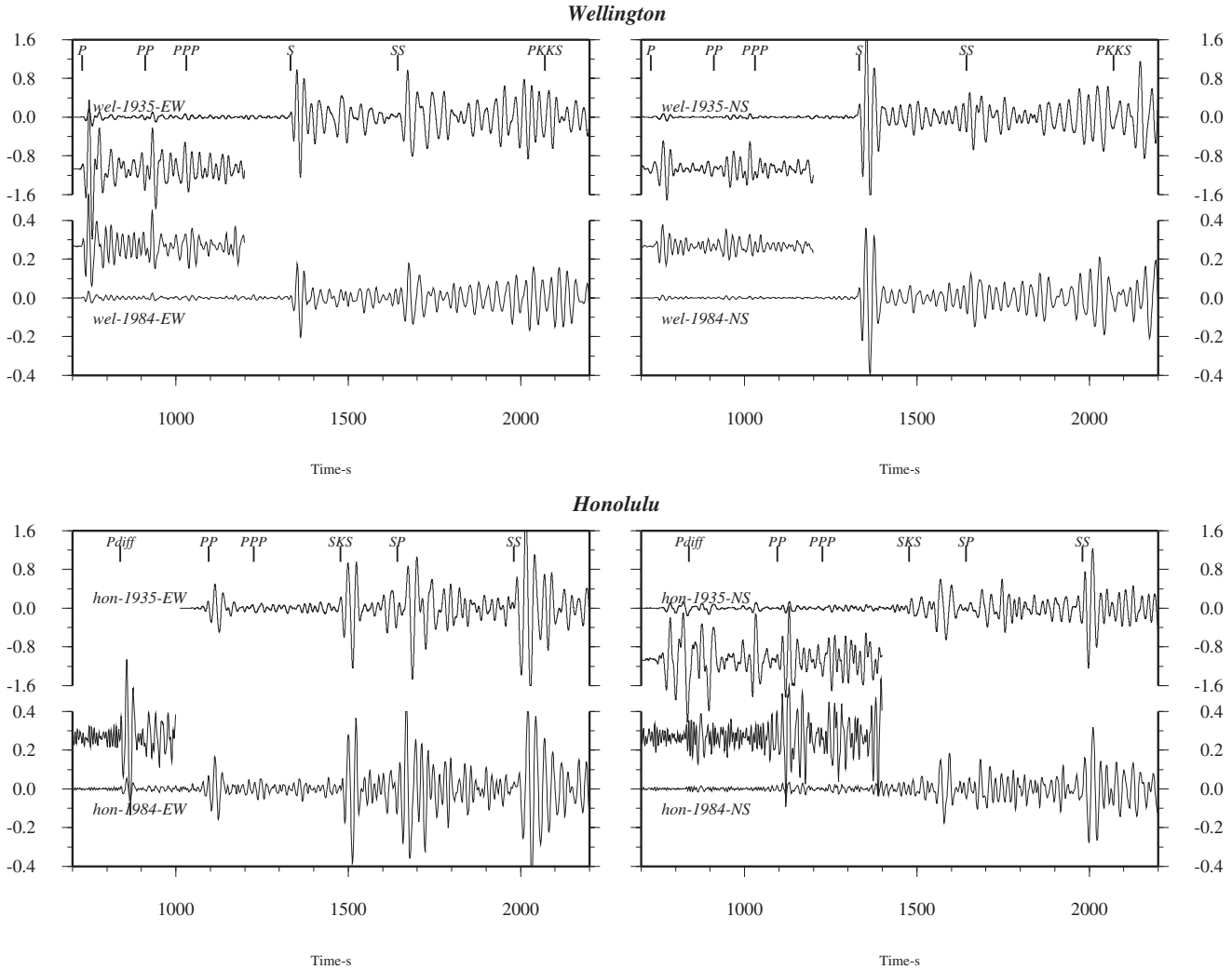

Figure 6. Reconvolved traces of the 1984 and 1935 events. For each station, four traces are displayed; in the top the two historical components (EW and NS) and in the bottom the two modern records. The traces corresponding to the 1984 event are plotted with a scale four times bigger than those of 1935, to better appreciate their similarity. Also, each trace is accompanied by an inset showing its first segment amplified eight times. The theoretical arrival times for different phases have been identified. (*Continued on next page.*)

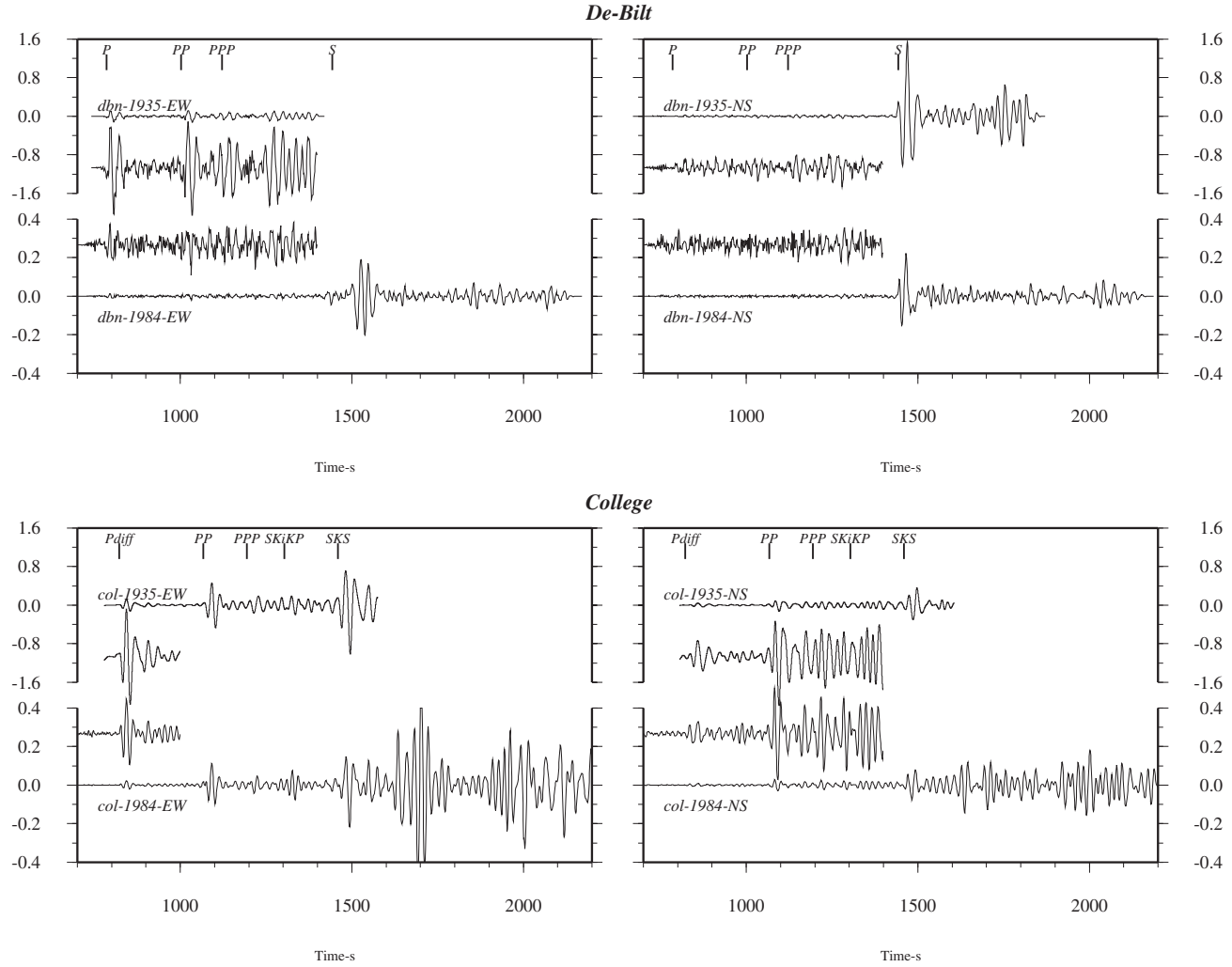

Figure 6. (*continued*)

shapes of those pulses, representing the source–time function, are relatively simple: they are more or less symmetric triangles with variable sizes. For those with a clear pulse, we measure the area and width. Figure 8a shows the area under the deconvolutions for all the phases and stations as a function of the azimuth. The mean value for the area under the pulses is 5.0 $\pm$ 1.0. This should be interpreted as the ratio between the two seismic moments. Thus, the event of 1935 has a seismic moment of 3.3 $\times$ 10^{20} N m (or M_w 7.7). The potency for the 1935 event, obtained from its moment, is 5.8 km^3. Five measurements (out of 25) are clearly anomalous. For three of these (col-N-P^{diff}, col-N-P^{diff}, and hon-N-S^{diff}) the reason could be a slight difference in depth for the two events. In fact, the waveforms of diffracted phases are extremely sensitive to slight variations in the path geometry. The striking stability of the ratio of the two moments, which is independent of the station or the phase, is a clear indication of the similarity between the two focal mechanisms. In particular, for the epicentral distances used here and the orientation of the focal spheres (Fig. 3), any slight variation of the dip of the mechanism will strongly affect the amplitudes and polarities of the phases leaving the source as *P*, whereas the *S* phases will be much less affected.

Figure 8b shows the relative duration of the source–time function. A mean value of 14 $\pm$ 2 sec results, with again the same three diffracted phases giving abnormal, longer pulses. To obtain the true source–time duration, we should add the duration of the 1984 event, used here as an empirical Green's function, to this value. We then obtain a duration for the 1935 event of 30 sec. Another piece of information that can be obtained from Figure 8 is the directivity of the rupture. Shorter and higher source–time functions at WEL indicate a unidirectional rupture toward this station, which happens to be nearly along strike of the fault plane (142°N versus 132°N; see Fig. 3). To estimate a rupture length by using the duration, we should assume a value for the rupture velocity. Extreme values reported for this parameter are 0.9 km/sec (Kikuchi and Fukao, 1987) and 4.5 km/sec (Fukao and Furumoto, 1975; Schwartz and Ruff, 1985). A more standard interval is probably 1.5–3.0 km/sec, which gives

lengths between 45 and 90 km; hereafter, we will use a value of 65 km.

Interpretation and Implications

Using the potency estimate of the 1935 event, we can attempt to disaggregate the three parameters that constitute it: fault length, width, and average displacement. Rupture length we have already estimated, by dividing the source duration into the rupture velocity. Disaggregation of the fault width and average displacement is more uncertain. For this, we need independent information, such as paleogeodetic data, to separate these two parameters. Absent such data, we must rely on scaling relationships derived from other earthquakes. Geller (1976), based on a dataset of 41 well-documented earthquakes, proposed an empirical scaling law for the aspect ratio of length to width for fault ruptures associated with moderate to large earthquakes. Geller's estimation for this aspect ratio is around 2, with a scatter of a factor of 2. If we use this relationship, we estimate a fault width of 30 km and are left with an average displacement D of about 3 m. This value is not well constrained; it depends strongly on the assumed rupture velocity and shape ratio of the fault. Supposing simultaneously extreme values for those parameters would give values for D as low as 1 m or as high as 10 m (and W of 90 or 9 km, respectively). The assumed values ($L = 65$ km, $W = 30$ km, and $D = 3$ m) correspond to a mean static stress drop of $\Delta\sigma \sim 60$ bars.

The location of the fault rupture can be constrained further. In addition to the seismological constraint on the geographic location of the hypocenter (Gutenberg and Richter, 1954), the down-dip limit of modern locking may correspond to the down-dip limit of the 1935 rupture. Sieh *et al.* (1999) uses paleogeodetic evidence from living corals, corresponding to the last three decades, to study the geometry of the present deformation regime. In particular, they estimate the horizontal distance from the trench to the lower edge of the down-dip locking region (x_{slip} in their notation) to be 133 ± 3 km. Thus, we suggest that the location of the 1935 rupture can be constrained to the location shown by the shaded rectangle in Figure 9, immediately up-dip from the base of the locked portion. In the northwest–southeast direction, we place the rupture using the seismologically determined hypocenter and the inference that rupture was unilateral toward Wellington (toward the southeast). In the northeast–southwest direction, we suppose the down-dip limit of rupture to be coincident with the paleogeodetically tightly constrained transition between locked and aseismically slipping portions of the subduction interface. Our estimate of a 30- to 35-km width for the rupture plane constrains the up-dip limit of rupture. The rectangle with the dotted perimeter in figure 9 indicates the northwest–southeast uncertainty in the location, due to the 1/4° uncertainty in the Gutenberg and Richter (1954) location.

Our best estimate of the location of the 1984 event also appears as a shaded rectangle in Figure 9, based solely on the seismologic data. The aspect ratio of the rectangle is 2:1, as suggested by Geller's survey of moderate to large ruptures. The open rectangle represents the uncertainty in the location; that is, the solid rectangle could float anywhere within the open rectangle. The uncertainty in location permits, but does not require, the 1984 event to be immediately up-dip from the base of the locked portion of the subduction interface.

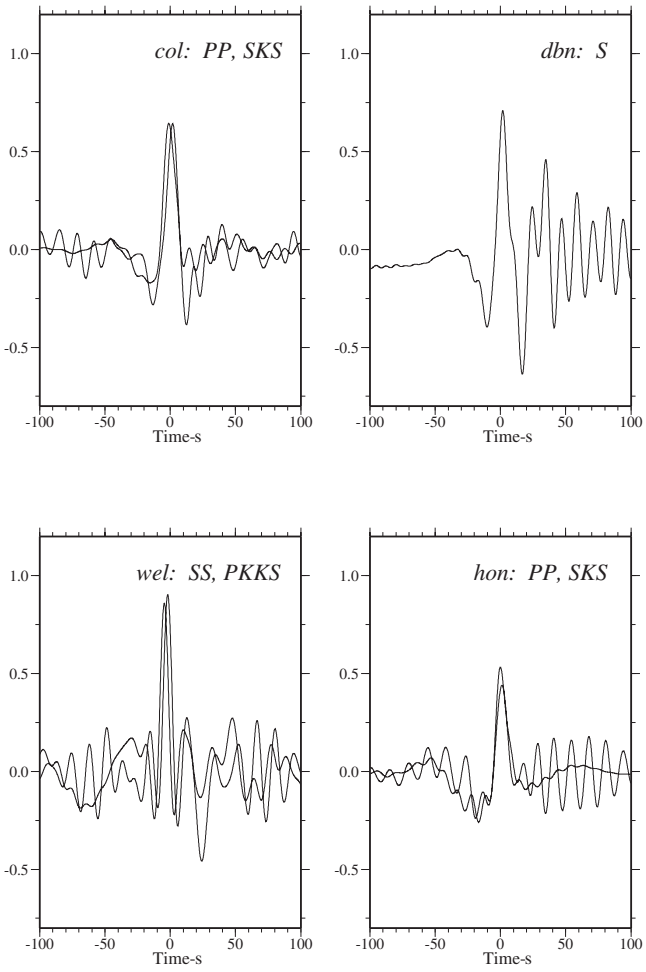

Figure 7. Deconvolutions (the result of deconvolving the traces of 1984 from those of 1935). The best deconvolutions for each station are shown.

Calculation of Surface Displacements

From the rupture parameters of the 1935 earthquake, we can estimate the magnitude and distribution of the coseismic surface displacements. Figure 10 displays our calculations of surface deformation for a finite fault with the source parameters estimated above. The parameters used in this calculation are as follows: length = 65 km, width = 30 km, dislocation = 3 m, hypocentral depth = 28 km, $\phi = 332°$, $\delta = 12°$, $\lambda = 108°$. The elastic structure used is the same multilayered half-space used above in modeling the body waves of the 1984 event. The finite source is simulated with an array of 20×10 point dislocations equally spaced on the surface of the equivalent rectangular rupture zone.

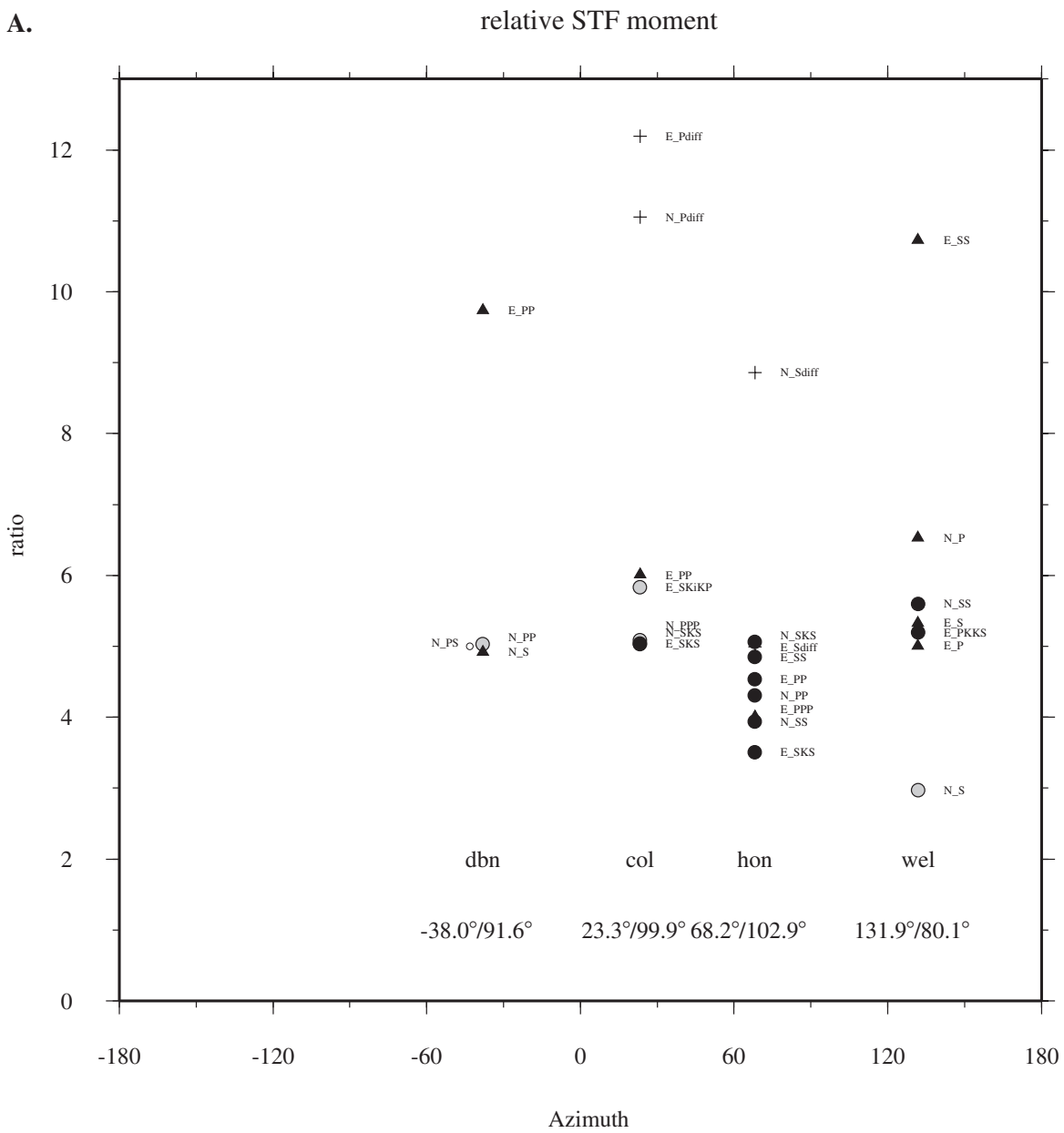

Figure 8. (a) Relative moment between the 1935 and 1984, as measured from the area under the main pulse on the deconvolutions, as a function of azimuth and (b) duration of the main pulse in the deconvolution as a function of the azimuth. The azimuth and epicentral distances are specified under the name of each station. Dark circles, dark triangles, and light circles indicate quality class A, B, and C, respectively. Crosses correspond to diffracted phases.

The primary features of the modeled surface displacement are adjacent elliptical regions of uplift and submergence. A maximum uplift of 70 cm occurs offshore, near the southwest coast of Tanabala Island. Maximum subsidence is only 35 cm just east of Tanamasa Island, and the distance between the two maxima is about 40 km. The slight asymmetry with respect to a ENE–WSW axis reflects the small component of strike-slip displacement. The region affected by vertical deformation large enough to be well recorded by the corals (10 cm, Zachariasen *et al.*, 2000) is approximately a rectangle of 80 by 80 km. Because of the uncertainties in the location of the 1935 event, the whole pattern can be in fact shifted in any direction by ~40 km. If our inclination to place the down-dip limit of rupture at the down-dip limit of modern locking is correct, the pattern can only shift northwest or southeast.

The validity of both the geographic placement of the rupture as well as its source parameters is testable, because

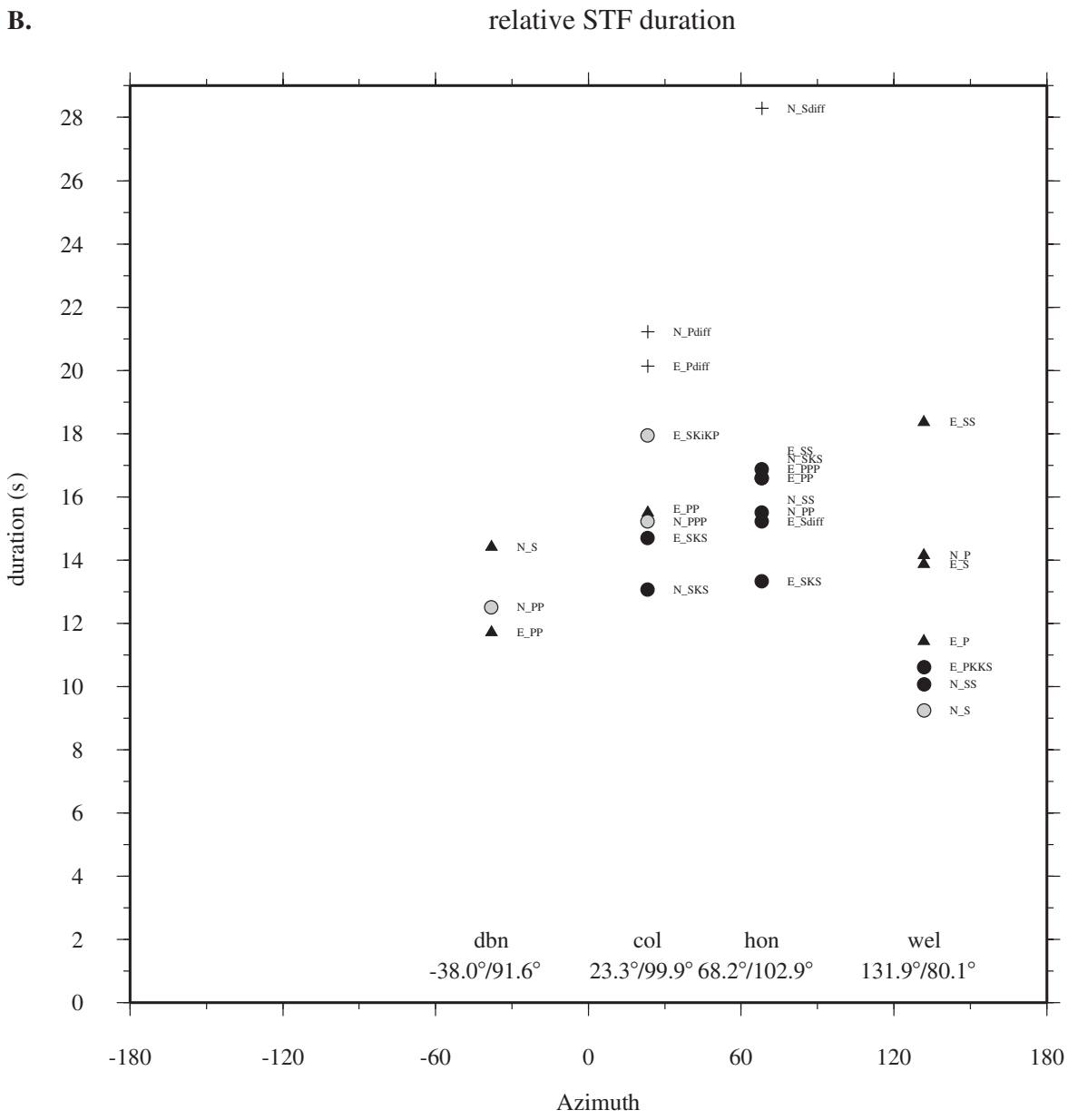

Figure 8. (*continued*)

we have collected corals from the region that were elevated and submerged during the 1935 earthquake. We are in the process of analyzing these samples. Regardless of the result of this paleoseismic study, the seismological constraints on the location and size of the 1935 earthquake suggest that the vertical deformation associated with the event is likely recorded by the corals around the Batu islands.

One final calculation that we can make concerns the average repeat time for earthquakes along this part of the Sumatran subduction zone. If we make the tenuous assumption that the 1935 earthquake is the typical seismic event here, we can calculate how often it must occur to relieve the accumulating relative plate motions. The component of relative plate motion parallel to the slip vector that we have calculated is 45 mm/yr. (The remaining vector component of the 65 mm/yr may be considered to be relieved by dextral slip along the Sumatran fault, 200 km to the northeast.) If all of the 45 mm/yr is relieved by 1935-type earthquakes, then such events would occur about every 70 years. The paleoseismic record from corals could reveal whether or not 1935-like events occur here with this frequency. Additionally, we might expect large ruptures on the subduction interface up-dip from the 1935 and 1984 ruptures. The fact that we have no evidence for such events in the past century or so suggests that slip is at least partially aseismic in this particular section of the subduction. Another possibility is that the giant adjacent earthquakes of 1833 and 1861 included the rupture regions of the 1935 and 1984 events.

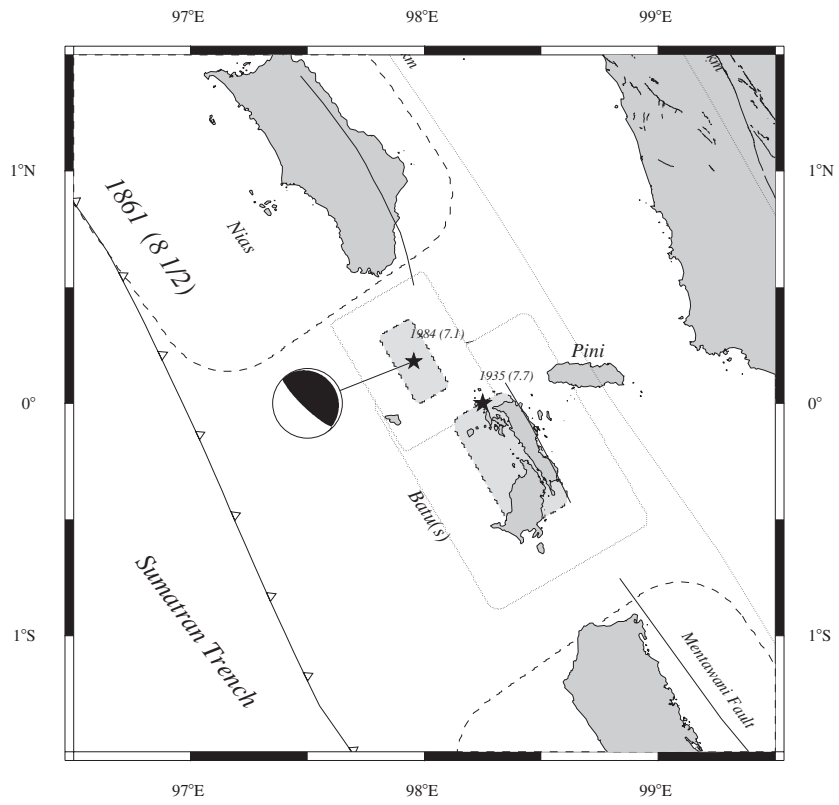

Figure 9. Likely geographic position and size of the rupture planes (shaded rectangles) for the 1935 and 1984 events, The estimated locations of the ruptures associated with the two giant earthquakes in the nineteenth century are modified from Newcomb and McCann (1987) and Zachariasen *et al.* (1999), based on more recent field work (in preparation). Open rectangles represent an estimate of the uncertainty in the location of the 1935 and 1984 ruptures.

Interpretation of GPS results from surveys conducted in the early 1990s suggests that, although the plate interface is wholly locked southward from about 1°S (Prawirodirdjo *et al.*, 1997), the interface is slipping for the most part aseismically in the region of the 1935 and 1984 earthquakes. The occurrence of the two earthquakes clearly demonstrates that the subduction interface is not completely aseismic. Therefore, either the behavior of the interface varies with time, or parts are seismically coupled while other parts are aseismically slipping.

Conclusions

In this study, we give an example of extracting quantitative information from historical seismograms by comparing them with records of a modern event. We obtain robust source parameters for the 1935 Sumatra earthquake, including its location, moment, mechanism, and surface deformation.

We first studied the 1984 event independently, to be used as an empirical Green's function for the 1935 event. The focal mechanism is a very shallow-dipping thrust fault, with a slip vector oblique to the convergence vector, but also oblique to the subduction direction. The seismic moment is 6.5×10^{19} N m (M_w 7.2), the source duration is about 16 sec, and the hypocentral depth is about 27 $\pm$ 2 km.

The waveforms generated by the 1935 and the 1984 Sumatra earthquakes are very similar. These two events appear to have occured within a few 10s of kilometers of each other and they have very similar mechanisms. They are located offshore of Sumatra, near the Equator, at the boundary between the two giant subduction earthquakes of 1833 and 1961. This is also the region where the Investigator Fault Zone obliquely intersects the subduction zone. The most energetic phases of the 1935 event, when deconvolved, reveal a simple source–time function, with a duration of 30 $\pm$ 2 sec and a seismic moment about five times larger than that of the 1984 event. The seismic moment for the 1935 event is 3.3×10^{20} N m (M_w 7.7).

Reasonable dimensions for the source of the 1935 earthquake are: length, 65 km; width, 30 km; and offset, 3 m. The vertical deformation pattern produced by such a rupture includes an elliptical region of uplift near the island of Tanabala of as much as 70 cm and an elliptical region of subsidence as great as 35 cm east of the island of Tanamasa.

The area affected by at least 10 cm of vertical deformation appears to be large enough to include the islands of Batu, even if we take into account the uncertainties in the location of the event. This event should thus be clearly visible in the paleogeodetic records of coral microatolls. The parameterization of the 1935 and 1984 earthquakes using seismic records can now serve as a basis for assessing the repeatability of large earthquakes in this region with paleoseismic methods.

Acknowledgments

We thank Hiroo Kanamori for many useful discussions throughout this study. Brian Ferris from the IGNS (New Zealand) and Torild Van Eck

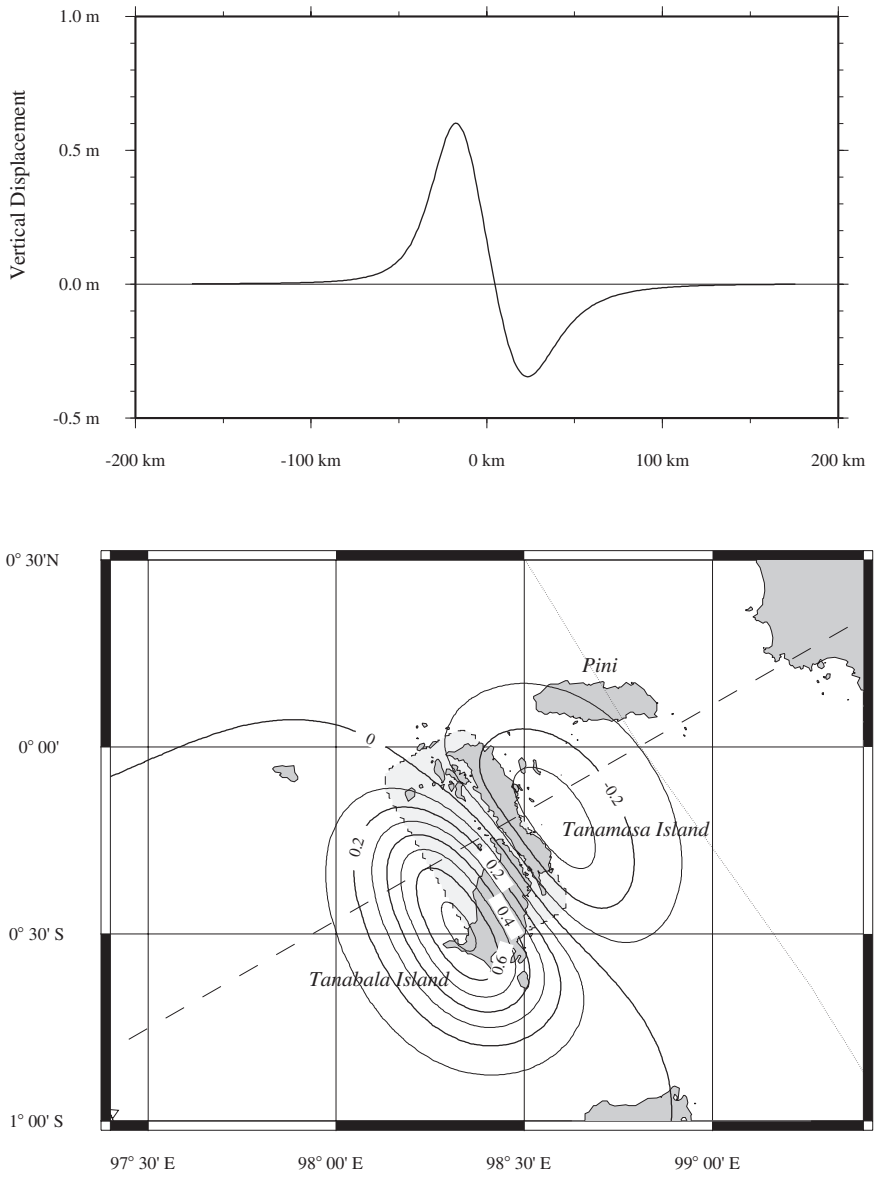

Figure 10. Surface deformation produced by the 1935 event, assuming these parameters: $L = 65$ km, $W = 30$ km, $H = 28$ km, $D = 3$ m, $\phi = 332°$, $\delta = 12°$, and $\lambda = 108°$ in a multilayered elastic half-space.

and Chris Meester from Orfeus/KNMI (Netherlands) kindly supplied some of the records used here. Anupama Venkataraman and Jascha Polet helped, reading and improving the manuscript. Dr. P. R. Cummins provided us with a thorough review and numerous comments and suggestions. This research was supported by the National Science Foundation Grant Number EAR 9903301. Contribution 8752, Division of Geological and Planetary Sciences, California Institute of Technology, Pasadena, California and 2002.17-UMR7516, EOST, Universite Louis Pasteur, Strasbourg, France.

References

Abercrombie, R. E., K. Felzer, M. Antolik, and G. Ekstrom (2000). The June 2000 Sumatera earthquakes (M 7.8): part of the India-Australia plate boundary? (abstract), *Eos Trans. Am. Geophys. Union* 81 (Fall Meet. suppl.), F913.

Beck M. E. (1991). Coastwise transport reconsidered: lateral displacements in oblique subduction zones, and tectonic consequences, *Phys. Earth Planet. Inter.*, **68,** 1–8.

Ben-Menahem, A., and S. J. Singh (1981). *Seismic Waves and Sources*, Springer, New York.

Bolt, B. (1968). The focus of the 1906 California earthquake, *Bull. Seism. Soc. Am.* **58,** 457–471.

Charlier, C., and J. M. Van Gils (1953). Liste des stations seismologiques mondiales, Observatoire Royal de Belgique, Uccle.

Cummins, P. R., T. Baba, S. Kodaira, and Y. Kaneda (2001). The 1946 Nankai earthquake and segmentation of the Nankai Trough, *Phys. Earth Planet. Inter.*, (in press).

Diament, M., H. Harjono, K. Karta, C. Deplus, M. T. Z. Dahrin, M. Gerard, O. Lassal., A. Martin, and J. Malaud (1992). Mentawani fault zone off Sumatra: a new key to the geodynamics of western Indonesia, *Geology* **20,** 259–262.

Doser, D., and W. A. Brown (2001). A study of historic earthquakes of the Prince William Sound, Alaska, region. *Bull. Seism. Soc. Am.* **91** 842–857.

Deplus, C., M. Diament, H. Habert, G. Bertrand, S. Dominguez, J. Dubois, P. Patriat, B. Pontoise, and J. J. Sibilla, (1998). Direct evidence of active deformation in the eastern India oceanic plate, *Geology* **26,** no. 2, 131–134.

Dziewonski, A. M., and J. H. Woodhouse, (1983). An experiment in systematic study of global seismicity: centroid-moment tensor solutions for 201 moderate and large earthquakes of 1981, *J. Geophys. Res.* **88,** no. B4, 3247–3271.

Dziewonski, A. M., J. E. Franzen, and J. H. Woodhouse (1985). Centroid-moment tensor solutions for October–December, 1984, *Phys. Earth Planet. Inter.*, **39,** 147–156.

Estabrook, C. H., K. H. Jacob, and L. R. Sykes (1994). Body waves and surface waves analysis of large and great earthquakes along the eastern Aleutian arc 1923–1993: implications for future events, *J. Geophys. Res.* **99,** no. B6, 11,643–11,662.

Engdahl, E. R., R. van der Hilst, and B. Raymond (1998). Global teleseismic earthquake relocation with improved travel times and procedures for depth determination, *Bull. Seism. Soc. Am.* **88,** 722–743.

Fauzi, R. McCaffrey, D. Wark, Sunaryo, and P. Y. Prih Haryadi (1996). Lateral variation in slab orientation beneath Toba Caldera, northern Sumatra, *Geophys. Res. Lett.* **23,** no. 5, 443–446.

Fitch, T. (1972). Plate convergence, transcurrent faults, and internal deformation adjacent to Southeast Asia and the western Pacific, *J. Geophys. Res.* **77,** 4432–4460.

Fukao, Y., and M. Furumoto (1975). Foreshocks and miltiple shocks of large earthquakes, *Phys. Earth Planet. Inter.* **10,** 355–368.

Geller, R. (1976). Scaling relations for earthquake source parameters and magnitudes, *Bull. Seism. Soc. Am.* **66,** 1501–1523.

Geller, R., and H. Kanamori (1977). Magnitudes of great shallow earthquakes from 1904 to 1952, *Bull. Seism. Soc. Am.* **67,** 687–598.

Gundmundsson, O., and M. Sambridge (1998). A regionalized upper mantle (rum) seismic model, *J. Geophys. Res.* **103,** 7121–7136.

Gutenberg, B., and C. F. Richter (1954). *Seismicity of the Earth*, Princeton Univ. Press, Princeton, New Jersey.

Hartzell, S., and D. Helmberger (1982). Strong-motion modeling of the Imperial Valley earthquake of 1979, *Bull. Seism. Soc. Am.* **72,** 571–596.

Haskell, N. (1964). Radiation pattern of surface waves from point sources in a multi-layered medium, *Bull. Seism. Soc. Am.* **54,** 377–393.

Heaton, T. H., and R. E. Heaton (1989). Static deformation from point sources and force couples located in welded elastic poissonian half-spaces: implications for seismic moment tensors, *Bull. Seism. Soc. Am.* **78,** 813–84.

Helmberger, D., P. G. Somerville, and E. Garnero (1992). The location and source parameters of the Lompoc, California, earthquake of 4 November 1927, *Bull. Seism. Soc. Am.* **82,** 1678–1709.

ISS (1946). International seismological summary for 1935, University Observatory, Oxford.

Kanamori, H. (1988). Importance of historical seismograms for geophysical research, in *Historical Seismograms and Earthquakes of the World*, W. Lee, H. Meyers, and K. Shimazaki (Editors), Symposium on Historical Seismograms and Earthquakes, IASPEI-1985, Tokyo, Japan, Academic Press, San Diego, California, 16–33.

Kieckhefer, R. M. (1980). Geophysical studies of the oblique subduction zone in Sumatra, *Ph.D. Thesis.* Univ. of California, San Diego.

Kikuchi, M., and Y. Fukao (1987). Inversion of long-period *P*-waves from great earthquakes along subduction zones, *Tectonophysics* **144,** 231–247.

Kikuchi, M., and H. Kanamori (1982). Inversion of complex body waves, *Bull. Seism. Soc. Am.* **72,** 491–506.

Kikuchi, M., and H. Kanamori (1986). Inversion of complex body waves: II, *Phys. Earth Planet. Inter.* **43,** 205–222.

Kikuchi, M., and H. Kanamori (1991). Inversion of complex body waves: III, *Bull. Seism. Soc. Am.* **81,** 2335–2350.

Lay, T., L. Burdick, and D. Helmberger (1984). Estimating the yields of the Amchitka tests by waveforms intercorrelation, *Geophys. J. R. Astr. Soc.* **78,** 181–207.

Macelwane, J. B., and F. W. Sohon (1932). *Introduction to Theoretical Seismology, Part II: Seismometry*, Wiley, New York.

McCaffrey, R. (1992). Oblique plate convergence, slip vectors, and forearc deformation, *J. Geophys. Res.* **97,** no. B6, 8905–8915.

McComb, H. E. (1931). A tilt-compensation seismometer, *Bull. Seism. Soc. Am.* **21,** 25–27.

Newcomb, K. R., and W. R. McCann (1987). Seismic history and seismotectonics of the Sunda arc, *J. Geophys. Res.* **92,** 421–439.

Okal, E. A. (1977). The July 9 and July 23, 1905 Mongolian earthquakes: a surface wave investigation, *Earth Planet. Sci. Lett.* **34,** 326–331, 1952.

Peters, J. H. (1939). Low-magnification attachment for a Milne–Shaw seismometer, *Bull. Seism. Soc. Am.* **29,** 341–343.

Prawirodirdjo, L., Y. Bock, R. McCaffrey, J. Genrich, E. Calais, C. Stevens, S. Puntodewo, C. Subraya, J. Rais, P. Zwick, and Fauzi (1997). Geodetic observations of interseismic strain segmentation of the Sumatra subduction zone, *Geophys. Res. Lett.*, **24,** 2601–2604.

Romberg, A. (1919). Theory of a non-tilt seismograph, *Bull. Seism. Soc. Am.* **9,** 135–139.

Savarensky, Y., and D. Kirnos (1955). *Elements of Seismology and Seismometry* (Translation from the Russian: *Elementy Seysmologii i Seismometrii*), GITTL, Moscow, 538 pp.

Sieh, K., and D. Natawidjaja (2000). Neotectonics of the Sumatran fault, Indonesia, *J. Geophys. Res.* **105,** 28,295–28,326.

Schwartz, S., and L. Ruff (1985). The 1968 Tokachi-Oki and the 1969 Kurile Islands earthquakes: variability in the rupture process, *J. Geophys. Res.*, **90,** no. B10, 8613–8626.

Sieh, K., S. Ward, D. Natawidjaja, and W. Suwargadi (1999). Crustal deformation at the Sumatran subduction zone revealed by coral rings, *Geophys. Res. Lett.* **26,** 3141–3144.

Sieh, K., J. Zachariasen, L. Edwards, F. Taylor, and P. Gans (1994). Active tectonics of Sumatra (abstract), Geological Society of America, 1994, Annu. Meet. A-382.

Wald, D., H. Kanamori, D. Helmberger, and T. Heaton (1993). Source study of the 1906 San Francisco earthquake, *Bull. Seism. Soc. Am.* **83,** 981–1019.

Zachariasen, J., K. Sieh, F. W. Taylor, R. L. Edwards, and W. S. Hantoro (1999). Submergence and uplift associated with the giant 1833 Sumatran subduction earthquake: evidence from coral microatolls, *J. Geophys. Res.* **104,** 895–919.

Zachariasen, J., K. Sieh, F. W. Taylor, and W. S. Hantoro (2000). Modern vertical deformation above the Sumatran subduction zone: paleogeodetic insights from coral microatolls, *Bull. Seism. Soc. Am.* **90,** 897–913.

Seismological Laboratory
California Institute of Technology
Mail Code 252-21
1200 E. California Blvd.
Pasadena, California 91125
(L.R., K.S., D.H., D.N.)

École et Observatoire des Sciences de la Terre
ULP-CNRS
5, rue René Descartes
67084 Strasbourg cedex
France
(L.R.)

Manuscript received 1 February 2001.